

Controlling Propagation Velocity in Al/Ni Reactive Multilayer Systems by Periodic 2D Surface Structuring

Yesenia H. Sauni Camposano,* Konrad Jaekel, Sascha S. Riegler, Sebastian Matthes, Marcus Glaser, Nicolas J. Peter, Emina Vardo, Heike Bartsch, Ruth Schwaiger, Jean Pierre Bergmann, Isabella Gallino, and Peter Schaaf


The chemical energy released as heat during the exothermic reaction of reactive multilayer systems has shown potential applications in various technological areas, e.g., in joining applications. However, controlling the heat release rate and the propagation velocity of the reaction is required to enhance their performance in most of these applications. Herein, a method to control the propagation velocity and heat release rate of the system is presented. The sputtering of Al/Ni multilayers on substrates with periodic 2D surface structures promotes the formation of growth defects into the system. This modification in the morphology locally influences the reaction characteristics. Tailoring the number of 2D structures in the substrate enables the control of the velocity and maximum temperature of the propagation front. The morphology of the produced reactive multilayers is investigated before and after reaction using scanning electron microscopy, transmission electron microscopy, and X-ray diffraction. In addition, the enthalpy of the system is obtained through calorimetric analysis. The self-sustained and self-propagating reaction of the systems is monitored by a high-speed camera and a high-speed pyrometer, thus revealing the propagation velocity and the temperatures with time resolution in the microsecond regime.

1. Introduction

Reactive multilayer systems (RMS) are metastable film architectures that consist of alternating nanolayers with strongly exothermic mixing behavior. A local energy pulse is able to initiate fast atomic diffusion at the interfaces between the layers. Consequently, the heat produced in the reaction zone will diffuse into the unreacted areas of the system, propagate the reaction, and thus generate a self-sustained and self-propagating reaction, until the reactants are consumed.^[1–3] The atomic composition, architecture, microstructure, and morphology of the system determine the characteristics of the propagation, like temperature profile and velocity.^[4–6] RMS, as a subgroup of energetic materials, have shown interesting characteristics for potential applications in diverse technological areas. Among them, their use as heat sources for joining applications and as ignitors has been extensively investigated.^[7–13] Recently, the successful use of the high

Y. H. Sauni Camposano, S. Matthes, E. Vardo, P. Schaaf
Chair Materials for Electrical Engineering and Electronics
Institute of Materials Science and Engineering
Institute of Micro and Nanotechnologies MacroNano
TU Ilmenau
Gustav-Kirchhoff-Str. 5, 98693 Ilmenau, Germany
E-mail: yesenia.sauni@tu-ilmenau.de

K. Jaekel, H. Bartsch
Electronics Technology Group
Institute of Materials Science and Engineering
Institute of Micro and Nanotechnology MacroNano
TU Ilmenau
Gustav-Kirchhoff-Str. 1, 98693 Ilmenau, Germany

 The ORCID identification number(s) for the author(s) of this article can be found under <https://doi.org/10.1002/adem.202302272>.

© 2024 The Author(s). Advanced Engineering Materials published by Wiley-VCH GmbH. This is an open access article under the terms of the Creative Commons Attribution License, which permits use, distribution and reproduction in any medium, provided the original work is properly cited.

DOI: 10.1002/adem.202302272

S. S. Riegler, I. Gallino
Institute for Metallic Materials
Saarland University
Campus C6.3, 66123 Saarbrücken, Germany

M. Glaser, J. P. Bergmann
Production Technology Group
Department of Mechanical Engineering
Institute of Micro and Nanotechnology MacroNano
TU Ilmenau
Gustav-Kirchhoff-Platz 2, 98693 Ilmenau, Germany

N. J. Peter, R. Schwaiger
Institute of Energy and Climate Research (IEK-2)
Forschungszentrum Jülich GmbH
52425 Jülich, Germany

I. Gallino
Department of Materials Science and Engineering
Metallic Materials
TU Berlin
Ernst-Reuter-Platz 1, 10587 Berlin, Germany

energy release rate in the synthesis of modern materials, like high entropy alloys and high-temperature compounds,^[14,15] as well as for on-chip technologies and the healing of thin films,^[16] has been reported. Moreover, its potential application for biological hazard neutralization,^[17] or as igniter to control signals in pyrotechnic devices, represents future possibilities for these functional materials.^[18]

The reaction behavior of Al/Ni RMS has been extensively investigated due to the high rate of heat release during its reaction under self-propagation conditions. The maximum temperature and the velocity of propagation are features that can be varied by changing the bilayer thickness or intermixing of the system.^[5,6,19] However, changing these parameters involves complex changes in the fabrication process. Therefore, many efforts have been reported aiming to control the heat release rate during the reaction by applying new methodologies. It has been demonstrated that by adding alloying elements into the multilayers it is possible to reduce or increase the propagation velocities of the reaction.^[20] Fritz et al. enabled slow propagation velocities by producing low-density compacts of multilayer particles.^[17,21] Danzi et al. investigated the effect of the substrates as microheat sinks to tailor the temperature and velocity of the propagation front.^[22] This investigation demonstrates the influence of the substrate thermal properties on the thermal behavior of the system. Arlington et al. successfully achieved a significant reduction in propagation velocity by combining heat dissipation through a substrate with ignition delays induced by a reaction propagating between particles in RMS.^[23] Besides, the substrate topography plays an important role in the resulting microstructure and morphology of the system, for the multilayers produced by physical vapor deposition (PVD). Rough substrates will influence the roughness of the Al/Ni multilayers and their interfaces;^[24] nanostructured substrates will promote the formation of reactive systems with lower density and porosity.^[25,26] It was shown that the presence of pores in the microstructure of the multilayers will decrease the velocity of propagation.^[26–29] However, the pores were randomly distributed in the microstructure, and the values of propagation velocities and temperature were different for each sample. RMS with textured surface topography will favor the propagation in the direction of the structures; this effect was attributed to the hole-like defects and disruptions produced in the microstructure.^[28] In a previous investigation, substrates with structured surfaces were used to fabricate RMS with defined structures.^[7,27] There, the impact of surface structuring on the velocity of propagation, on the formation of cracks in the reacted material, and on the adhesion to the substrate was investigated. However, a quantitative analysis of the impact of the growth defects and porosity on the velocity of propagation and a deeper analysis of their impact on the dynamics of the reaction are still missing.

This research proposes a methodology for controlling the velocity and temperature of the self-propagating reaction of Al/Ni RMS by using substrates with periodic trench structures. These 2D structures affect the growth of Al/Ni nanolayers in systematically distributed areas, thereby modifying the morphology of the RMS, named RMS-T. The impact of the substrate surface on the morphology of the RMS-T and its consequent influence on the propagation features are investigated, with the aim to elucidate its influence quantitatively by the use of analytical models.

The characterization of the system before and after the reaction was carried out by scanning electron microscopy (SEM), scanning transmission electron microscopy (STEM), and X-ray diffraction (XRD). The enthalpy of the RMS was obtained by employing differential scanning calorimetry (DSC). During the reaction of the samples, the propagation behavior and the temperature were recorded by a high-speed camera and a high-speed pyrometer, respectively.

2. Experimental Section

2.1. Sample Preparation

In order to modify the morphology of the RMS-T in a controlled manner, Si chips with defined number of parallel trenches on the surface were used as a substrate. The trench structures were fabricated by using photolithography, reactive ion etching (RIE), and wet chemical etching, according to the procedure described by Jaekel et al.^[27] Prior to the photolithography process, a layer of SiO₂ with a thickness of 235 nm was grown by thermal oxidation on the surface of the n-type silicon wafer <100>. Due to the hydrophilic surface of the substrate, hexamethyldisilazane (HMDS) priming was required to promote the adhesion between the SiO₂ and the photoresist; in this process, the Si/SiO₂ wafer went through a dehydration bake at 105 °C for 30 min, and was subsequently exposed to vapor HMDS. The positive photoresist AZ1518 (Microchemicals GmbH) was applied on the surface by spin coating at a spinning speed of 4000 rpm during 60 s, and it was prebaked at 105 °C for 60 s. The exposure was carried out at a dose of 200 mJ cm^{−2} using a chrome mask with the patterns to produce the trench structures in the mask aligner MA8 (Süss MicroTec). Later the AZ developer (Microchemicals GmbH), diluted in water (1:1), was used for 35 s for the development. The RIE of the SiO₂ was performed in the Oxford RIE Plasmalab 100. The flow rates of the gases were 12 and 38 sccm for CHF₃ and Ar, respectively. The chamber pressure was set to 30 mTorr and the applied power was 200 W. This process was carried out for 10 min to remove the 235 nm of SiO₂. As a result, a surface with trench structures was produced. The next step was to remove the photoresist using acetone, isopropanol, and deionized water. In order to increase the depth of the obtained trenches, KOH etching was performed using an etching solution composed of 40% KOH. The temperature and the process time were 90 °C and 60 s, respectively. During the etching, a slope of 54.7° was expected due to the <100> orientation of the etched Si, as shown in **Figure 1a**. Finally, a second oxidation process was performed for 3 h to produce 1 μm of SiO₂ on the surface of the structured substrate. This layer will act as a thermal barrier, to reduce heat loss to the substrate during the reaction of the RMS. The trench width (13.8 μm) and trench depth (0.7 μm) were kept constant for all samples, while the number of trenches on the surface of the substrate varied as shown in **Table 1**.

The deposition of the multilayers was carried out using the PVD Cluster tool CS400 (Ardenne GmbH), employing direct current magnetron sputtering. The coating chamber boasts three magnetron sources strategically arranged in a confocal configuration (top-down sputtering); hence, this setup enables the deposition of various layer systems. The targets are tilted at a

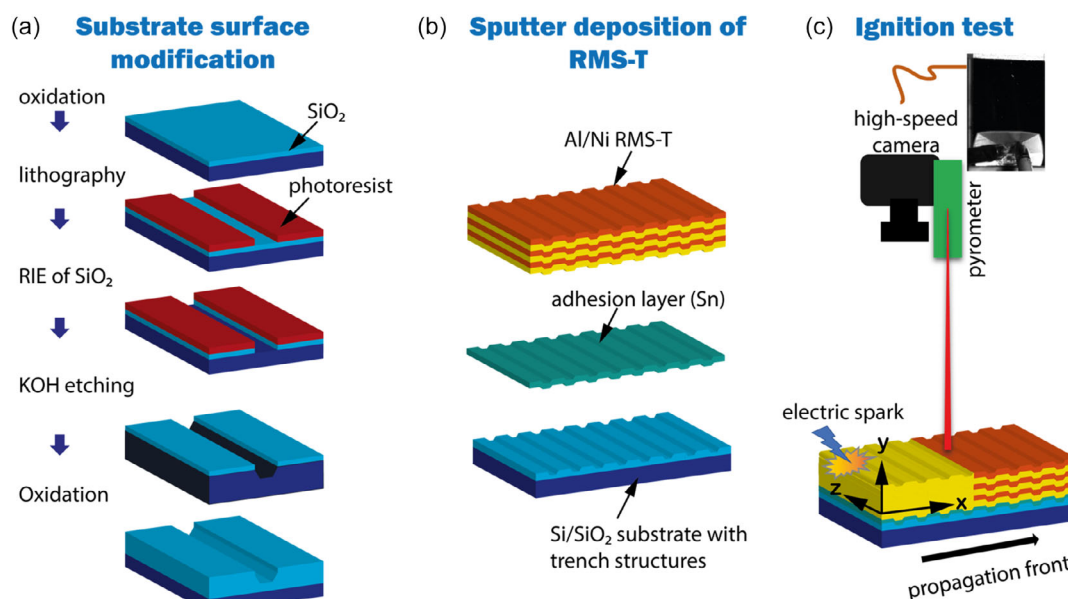


Figure 1. A schematic view (not on scale) of the fabrication process and the subsequent ignition test: a) substrate surface modification; b) sputtering fabrication of the RMS-T; and c) ignition of the RMS-T by an electric spark. The coordinate system points directions normal to the Al/Ni layers (y), normal to the trenches (x), and parallel to the trenches (z).

Table 1. Experimental setup for the variation of the trenches on the surface of the Si/SiO₂ substrate and the bilayer thickness Λ for the produced samples.

Sample name		Substrate SiO ₂ /Si	#trenches [1 cm ⁻¹]	Distance between trenches [μm]
$\Lambda = 20$	$\Lambda = 50$			
RMS20-Reference	RMS50-Reference	Reference	0	–
RMS20-T27	RMS50-T27	T27	27	350
RMS20-T71	RMS50-T71	T71	71	125
RMS20-T153	RMS50-T153	T153	153	50
RMS20-T333	RMS50-T333	T333	333	15
RMS20-T500	RMS50-T500	T500	500	5

40° angle relative to the sample holder, with the midpoint of the targets positioned ≈ 104.5 mm from the midpoint of the sample holder. The structured substrates, measuring 15×10 mm, were positioned on the sample holder with a diameter of 100 mm. This enabled the simultaneous deposition of multilayers on 24 samples (4 for each configuration). Throughout the deposition process, each magnetron source will dynamically adjust its power output as required. Additionally, to prevent contamination, a shutter will automatically cover the target when it is not in use. The substrates were placed into the vacuum chamber, where a base pressure of 5×10^{-5} Pa and a residual gas pressure of 1.6×10^{-4} Pa were achieved. To improve the adhesion of the multilayers to the substrate surface, 50 nm of Sn was deposited as a first layer. Subsequently, Al and Ni layers were produced. The process was carried out at room temperature, with a working pressure of 5×10^{-1} Pa, while the sputtering power and the argon flow were set to 200 W and 30 sccm, respectively.

The transition time between the deposition of Ni and Al, and vice versa, is ≈ 10 s. Throughout this transition, parameters such as argon flow and pressure remained constant. Pressure regulation within the system was achieved through a proportional integral derivative controller, which modulates the opening of the active butterfly valve situated between the vacuum pump and the chamber, ensuring pressure stability. The process was carried out employing Al (99.99% purity, FHR) and Ni (99.99% purity, FHR) targets, resulting in a deposition rate of 0.32 nm s^{-1} for Al and 0.26 nm s^{-1} for Ni. Using these parameters, alternating layers of Al and Ni were grown on the substrate, until reaching a total thickness of $T_{\text{th}} = 5 \text{ μm}$; the individual thickness of the layers was calculated in order to achieve an atomic ratio of 1:1 between Al and Ni. The first batch of samples was produced with a bilayer thickness of $\Lambda = 20$ nm (Al layers of 12 nm and Ni layers of 8 nm thickness) and the second batch with $\Lambda = 50$ nm (Al layers of 30 nm and Ni layers of 20 nm thickness). Each batch of samples also includes RMS deposited on Si/SiO₂ chips without any trenches. These will be referred to as reference samples.

2.2. Analysis Methods

The microstructural features of the Al/Ni RMS-T before and after the reaction were investigated by SEM and STEM. Top-view images were obtained using SEM (S-4800 HITACHI) with an operating voltage of 5 kV. STEM lamellae were prepared to obtain cross-sectional views using a Xe ion plasma focused ion beam machine (Thermo Fischer Scientific), to avoid influences from more common Ga using machines in Al-containing material systems. A standard lift-out procedure was finished with a final lamella polishing step using a 5 kV accelerating voltage to reduce ion beam-induced damage as much as possible. STEM was

carried out at 200 kV acceleration voltage and with a 24.7 mrad convergence angle in an aberration-corrected Titan G² 60-200 CREWLEY microscope (Thermo Fischer Scientific). High-angle annular dark field (HAADF) STEM images were acquired at a semicollection angle of 69–200 mrad to make use of the associated mass-thickness contrast.

In order to identify the crystalline phases in the produced RMS-T, before and after the reaction, the samples were examined by XRD. The scanning of the samples was carried out in Bragg–Brentano mode at speed of 1 s per step and using sampling steps of 0.02°, using a Bruker D5000 Theta–Theta XRD, equipped with a Cu K α ($\lambda = 0.15418$ nm) radiation source operated at 40 kV and 40 mA. The software package Bruker DIFFEAC.EVA V5.1 was used for the analysis of the obtained diffraction data. Furthermore, calorimetric investigations of the as-deposited RMS-T were carried out with a power-compensated Perkin Elmer Differential Scanning Calorimeter 8500 using Al pans under a constant high-purity Ar flow (99.9999 vol%) of 20 mL min^{−1}. Free-standing thin films of the RMS-T were obtained by peeling the thin film from the substrate mechanically. In order to provide enough mass (≈ 1.8 mg) for a good signal-to-noise ratio, several cuts of the free-standing RMS-T were used. The free-standing samples were continuously heated from 300 to 853 K with a constant rate of 0.333 K s^{−1}. A second run with the reacted material under identical conditions was used to determine baselines that could be subtracted from the first up-scan.

During the ignition test, the chemical reaction of the Al/Ni RMS-T was activated by an electrical spark. The tests were carried out in air and at room temperature. The propagation front was recorded using a high-speed camera (FASTCAM SA-X2 type 480 K) with a time resolution of 50 000 fps. At the same time, the temperature was measured by a high-speed pyrometer (KLEIBER-Pyrometer Pyroskop 840), where the emissions coefficient value (ϵ) was fixed to 0.3 and the resolution time to 10 μ s. We note that assuming a single emission coefficient value during the reaction process may result in deviations from the actual temperature values. This is because emissivity is influenced by temperature fluctuations during the reaction, as well as variations in surface properties resulting from the transformation from unreacted to reacted material. However, due to the complexity of the process, it is used solely for comparison purposes. In all the produced multilayers, a Ni layer was in the exterior. The emissivity of Ni at high temperatures was reported between 0.2 and 0.33,^[30] while for AlNi, it was reported between

0.25 and 0.35.^[31] Therefore, we chose 0.3 as a reasonable value for the emission coefficient. The measuring point of the pyrometer has a diameter of 400 μ m and was located in the middle of the sample. The velocity of the reaction propagation was measured in x -direction, as shown in Figure 1, by using the obtained videos in combination with the tool “manual tracking” with the software Image J.^[32]

3. Results

3.1. Characterization of the RMS-T Morphology

The multilayers grown on the structured substrates were investigated using SEM and TEM. The obtained micrographs of the surface and the cross section of the RMS are shown in Figure 2, where it can be observed that the trench structures on the surface of the substrate were adopted by the multilayers, producing RMS with trenched structures (RMS-T). However, in the flanks, film discontinuities in the form of thin holes, which extend from the substrate to the top surface of the RMS-T, can be observed. These defects are known as pinholes and it is one of the most common growth defects in PVD thin films.^[33] Due to the shadowing effect, the deposition rate on the flanks of the trenches is much lower in comparison with the deposition rate in the flat areas of the surface.^[34,35] Furthermore, it is expected that the film grown on the flanks has a columnar and porous structure.^[35] A closer view was possible using STEM (Figure 2c,d), which shows that even in the flanks a uniform distribution of the Al/Ni layers could be obtained. However, the bilayer thickness of the RMS-T on the flanks is 37 nm on average, which differs from the nominal 50 nm bilayer thickness on the flat areas. The shadowing effect influences not only the growth of the thin layers in the flanks, but also the layers in the neighboring areas. The red rectangle in Figure 2c frames the region in the RMS-T that was affected by the shadowing effect during the deposition of the Al/Ni layers. In this region, growth defects, like bilayer thickness variations and pinholes, could be observed. This growth-defect region is 1.5 μ m in the longitudinal plane of the RMS-T.

It is anticipated that parameters such as the depth of the trenches and the slope of the flanks will affect the shadow effect, thereby influencing the characteristics of multilayers within the growth-defect region and consequently impacting the formation of pinholes. Preliminary experiments have demonstrated that larger pinholes could halt the self-propagation process. Further investigation will be conducted to customize pinholes

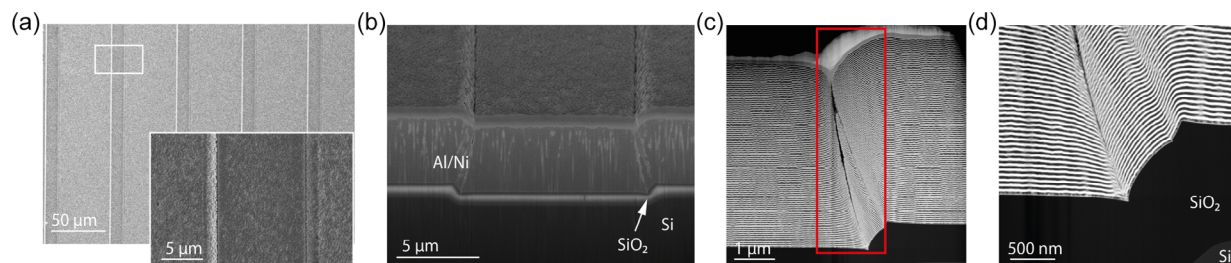


Figure 2. SEM and TEM micrographs of the RMS-T ($T_{th} = 5$ μ m, $\Lambda = 50$ nm); a) surface (SEM); b) cross section of a trench structure (SEM); c) growth defects on the trench structure flank (HAADF-STEM), the red rectangle frames the growth-defect region; and d) closer view of the Al/Ni layers on the flank of a trench structure (HAADF-STEM).

and other defects in the multilayers by utilizing structured substrates.

3.2. DSC Analysis

The DSC measurements were carried out for flat RMS (reference sample) and RMS-T with a heating rate of 0.333 K s^{-1} . The mechanical peeling of the multilayers from the substrate while maintaining their structural integrity was a challenging process and not always successful. During peeling, the multilayers tended to crack and break. Consequently, it was only possible to obtain enough material for one measurement for each sample configuration, except for the RMS-T333 where the mechanical peeling was not possible due to the high adhesion of the multilayers to the substrate. In contrast, the reference sample allowed for relatively easy mechanical peeling, enabling three measurements to be performed. The obtained heat flow curves as a function of temperature are shown in **Figure 3**. The heat flow behavior of the reference samples and the RMS-T were found to be similar because the exothermic peaks are observed at the same temperatures. These exothermic events were observed in multiple studies for the transformation of Al/Ni multilayers to AlNi (B2 phase) at low heating rates.^[17,36,37]

The average enthalpy release for the reference samples is $-50.3 \text{ kJ g-atom}^{-1}$ with a standard deviation of $0.75 \text{ kJ g-atom}^{-1}$. The enthalpy for the RMS-T27, RMST71, and RMST 153 is -50.04 , -49.4 , and -52.7 kJ , respectively. These values closely approximated to those obtained for the reference sample, while, for the RMS-T500, the calculated enthalpy is $-57.3 \text{ kJ g-atom}^{-1}$. Given the limited number of samples studied, it is not feasible to draw any meaningful conclusions regarding the variation of enthalpy at this juncture. However, changes in the diffusion process may be attributed to the distinct characteristics of the multilayers in the growth-defect region (refer to Figure 2c). In the cases of RMS-T27, RMS-T7, and RMS-173, the growth-defect

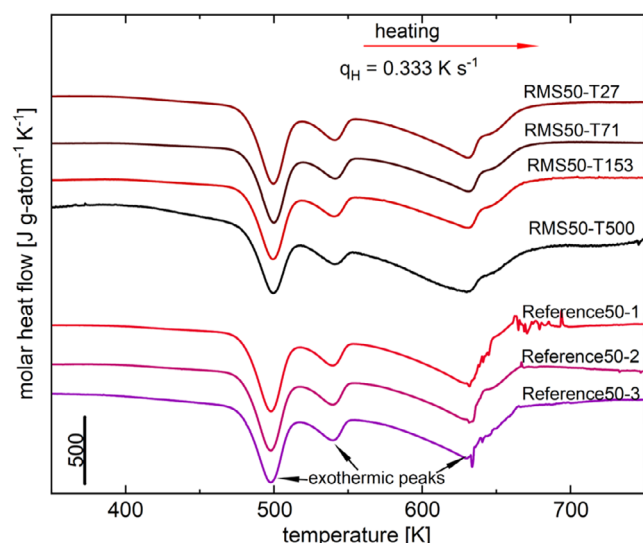


Figure 3. Heat flow from DSC scans of Al/Ni RMS-T ($\Lambda = 50 \text{ nm}$) conducted at 0.333 K s^{-1} , where the molar heat flow is plotted versus temperature.

region constitutes less than 5% of the total volume of the system, showing no discernible impact on the heat release behavior or enthalpy under solid–solid diffusion conditions; thus, it can be considered negligible. For RMS-T500, the percentage of multilayers affected by the shadow effect and the flank of the trenches already represents 15%. Differences in bilayer thickness, columnar growth, and porosity influence the atomic diffusion behavior and therefore the heat release.^[5,24,37] Therefore, it could be expected that when the volume of the growth-defect region in the system increases significantly, it could impact the heat release behavior and the enthalpy of mixing.

3.3. Self-Propagating Reaction

The reaction of the Al and Ni layers was promoted by spark ignition and the velocity of the propagation front is measured in perpendicular direction to the trench structures (x -direction). The impact of the trench structures on the propagation front of the reaction is shown in **Figure 4**. The pictures were extracted from the videos recorded by the high-speed camera 0.5 ms after local ignition. The radial propagation front of the reaction of multilayers deposited on flat substrates was already observed and intensively investigated.^[38,39] However, the propagation front of the RMS deposited on textured surfaces was recently presented.^[27,28] In preliminary experiments, it was observed that the propagation of the reaction was favored in the direction parallel to the trenches (z -direction), while in the perpendicular direction (x -direction), the propagation slowed down. Similar effects were observed when RMS was deposited on copper substrates with textured surface topography.^[28]

3.3.1. Propagation Velocity v_{prop} and Maximum Temperature T_m

By using the high-speed camera videos, the velocity of propagation v_{prop} (in x -direction) was calculated for each sample. The values of v_{prop} calculated for RMS20 and RMS50 are 19.4 and 10.4 m s^{-1} , respectively. These results show the influence of the bilayer thickness on v_{prop} . Kneeples et al. attributed this effect to the change in the diffusion distance.^[19,36] As the thickness of the bilayer increases, so does the diffusion distance for atoms within Al and Ni layers. Consequently, this longer diffusion path slows down the propagation velocity. In order to decouple the impact of the trench structures and the bilayer thickness, batch 1 ($\Lambda = 20 \text{ nm}$) and batch 2 ($\Lambda = 50 \text{ nm}$) are analyzed separately. The plot of v_{prop} and T_m values in relation to the number of trench structures per centimeter is shown in **Figure 5**; this allows a better visualization of the influence of the trench structures on the characteristics of the propagation front.

For the RMS-T with $\Lambda = 20 \text{ nm}$, the velocity of propagation varies from 19.4 to 7.3 m s^{-1} and the maximum temperature varies from 1722 to 1560 K . When the reaction propagation occurs normal to the trenches, the plot shows a clear decrease in the maximum temperature and the propagation velocity, while the temperature decreases rather linearly, the velocity decreases exponentially in relation to the number of trench structures per cm. As expected, a similar trend was observed for the multilayers of 50 nm bilayer thickness, the velocity varied from 10.4 to 4.5 m s^{-1} , and the temperature from 1097 to 1008 K . It must

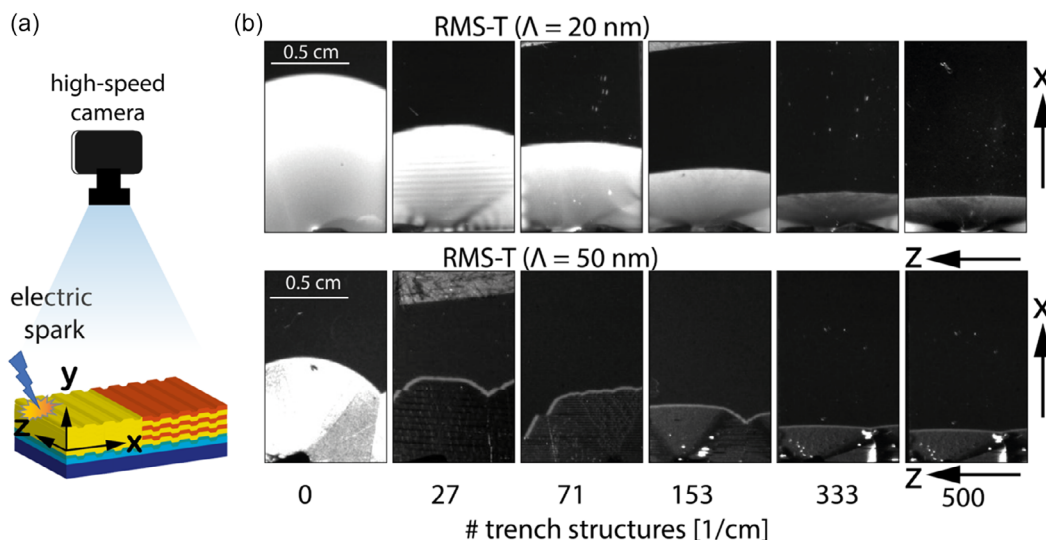


Figure 4. a) Schematic view of the ignition test and b) images of the propagation front obtained by the high-speed camera in intervals of 0.5 ms after the ignition; upper pictures RMS-T with 20 nm bilayer thickness and lower pictures RMS-T with 50 nm bilayer thickness. The videos can be found in Zenodo (<https://zenodo.org/records/10436346>).^[47] The trench structures are aligned to z-direction.

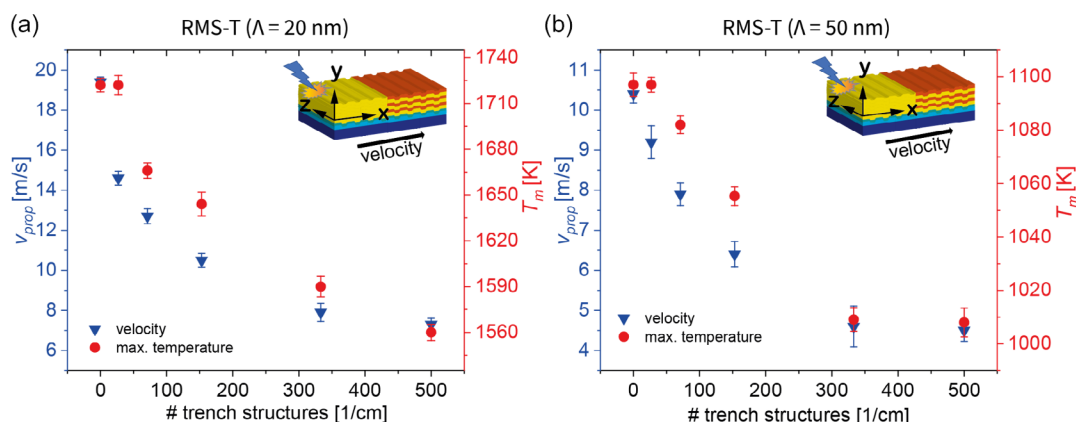


Figure 5. Plot of the velocity of propagation (in x-direction) and estimated maximum temperature versus the number of trench structures per cm: a) RMS-T with $\Lambda = 20$ nm and b) RMS-T with $\Lambda = 50$ nm (error bars indicate the standard deviation of three samples per data point).

be noted that the monitored temperatures are only approximations of the real ones because the emission coefficient ϵ was set to a single value of 0.3, assuming a constant emissivity during the reaction. The increase of the path for the propagation front due to the trench structures was calculated for each sample, and its impact on the calculated velocity was found negligible. Jaekel et al. described in detail this analysis for similar structures.^[27]

Unlike the multilayers with 20 nm bilayer thickness, the multilayers with 50 nm bilayer remained attached to the substrate surface after the reaction. **Figure 6** depicts the monitored temperature values as a function of time. There is a clear trend visible for the heating rate, peak high, and peak time dependent on the number of trenches. The effects of structured substrates on the velocity of propagation and heat release rate were recently presented and were attributed to the defects in the microstructure of the system.^[26,28] The generation of a defined defect zone with a defined orientation to the reaction front allows a qualitative

discussion. However, a quantitative analysis of the total amount of heat release is not possible because different factors could affect the temperature measured at the sample surface, e.g., heat loss to the substrate, crack formation, and micro-delamination. Additionally, due to the abovementioned conditions, ϵ must be adjusted.

3.4. Characterization after Reaction

XRD analysis was conducted before and after ignition. The XRD patterns obtained from the parent layers revealed reflections corresponding only to fcc Al and fcc Ni. After the reaction, despite changes in the heat release rate and the impact of trench structures on the propagation front, the Al and Ni layers consistently formed the B2 AlNi phase in all reacted samples. This demonstrates that the change in the heat release rate does not affect the complete transformation of the parent material.

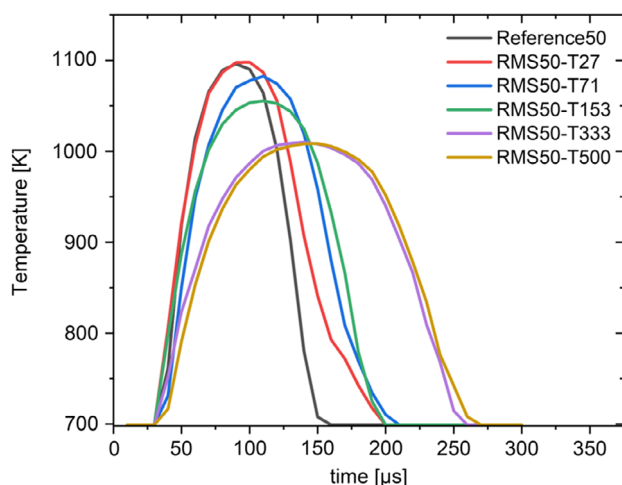


Figure 6. Temperature–time curves $T(t)$ recorded by using the high-speed pyrometer during the reaction of RMS-T with a tailored number of trench structures ($\Lambda = 50$ nm).

Flash calorimetry or in-situ XRD investigations are necessary to elucidate the changes in the phase transformation process under self-propagation conditions.

The surface of the reacted samples was investigated using SEM. In **Figure 7**, the appearance of cracks can be seen. The formation of cracks after the reaction of the Al/Ni system was already reported and it is attributed to the volume shrinkage, which occurs due to the increase of the density of the resulting AlNi of about 12% compared to the average density of the parent materials.^[7] Figure 7a–f shows the influence of the distance between the trenches on the size and distribution of the cracks. A closer view in Figure 7g allows observation of the cracks formed at the trench flanks, where the growth defects were located. When the distance between the trench structures is equal or less than $50\ \mu\text{m}$, the cracks will form in a systematic order only at the flanks and perpendicular to them, while in the reference sample Figure 7a, the cracks propagate in a radial

direction from the ignition point. These observations indicate that the introduced growth defects promote the formation of cracks in specific areas to compensate the volume change. Further investigation using TEM is necessary to elucidate the impact of the variation of T_m and v_{prop} on the grain morphology of the reacted RMS-T.

4. Discussion

4.1. The Effect of the Produced Growth Defects on the Maximum Temperature

For an ideal system, the heat produced during the exothermic reaction of Al and Ni will dissipate to the unreacted regions of the foil, generating a self-propagating wave. The amount of heat depends on the atomic composition, bilayer thickness, and its microstructural characteristics.^[5,40] In the produced samples, during the reaction of the system, the heat loss to the substrate and to the surroundings will decrease the amount of heat available to be transferred to the unreacted areas.^[22] Therefore, the values of temperature and velocity obtained during the reaction of RMS-T deposited on structured SiO_2 are compared with the results obtained for the RMS deposited on flat SiO_2 substrate (reference sample). The impact of the bilayer inhomogeneities in the enthalpy of the system was found to be negligible. Therefore, the decrease in the maximum temperature during self-propagation can be attributed, mainly, to the impact of the pinholes on the thermal diffusion. These defects will act as barriers to the chemical and thermal diffusion, limiting the heat transport in the system.^[25,27] It is expected that in local areas, next to the pinholes, the energy available to promote the reaction is reduced, impacting the kinetics of the reaction, reducing the reaction rate and the peak of temperature.^[17,41] This agrees with the observation in Figure 6, where the maximum temperature tends to decrease, while raise time and peak time tend to increase with increasing number of trenches that correlate with a higher number of pinholes to be hurdled. In the case of the RMS-T27, the distance between the trenches is about $320\ \mu\text{m}$; consequently,

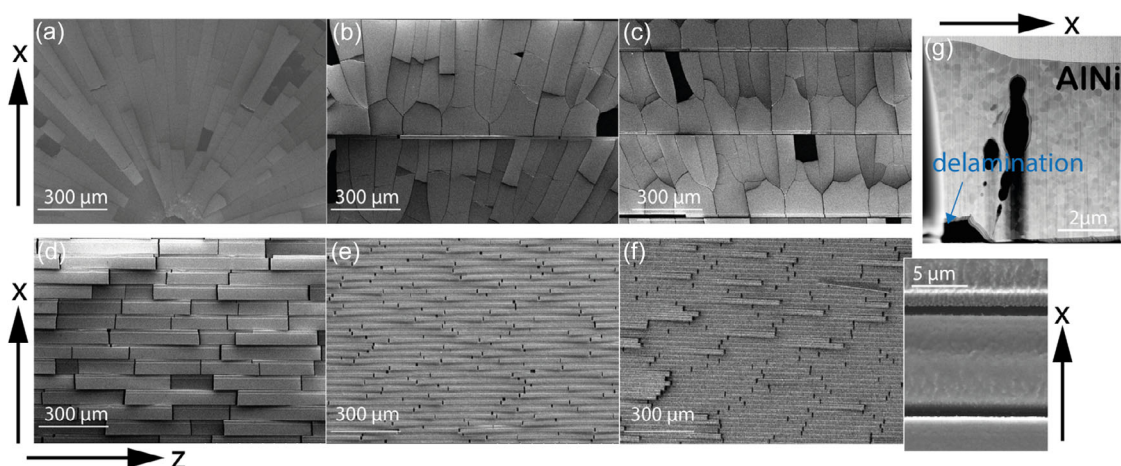


Figure 7. Crack formation after the reaction of RMS-T: a) reference sample; b) RMS-T27; c) RMS-T51; d) RMS-T153; e) RMS-T333; f) RMS-T500; the inset shows the top view of the cracks formed in the defect region of RMS-T500; and g) cross section of the defect region of RMS-T153 (STEM). Trenches parallel to z-direction and propagation front in x-direction.

this is the distance between pinholes. The maximum temperature, in this case, is similar to the reference sample, which indicates that 320 μm is enough for the system to return to steady-state propagation and reach the maximum temperature until the next defect is encountered, thus generating an oscillatory front. However, if the distance between the pinholes is 50 μm or less (RMS-T153), the heating rate is clearly affected, and the maximum temperature decreases in comparison with the reference sample. This fact could be exploited to influence the reaction rate and heat release behavior in the RMS by changing the distance between the introduced growth defects. Further investigations are necessary to quantify the impact of growth defects shape and size on the heat transfer and on the kinetics of the reaction.

4.2. Impact on the Propagation Velocity

The self-propagation process of the RMS in the shape of free-standing foils is mainly governed by atomic diffusion and thermal diffusion.^[1,37] The atomic diffusion, occurring perpendicular to the layers, drives the heat generation, while the thermal diffusion, predominantly parallel to the layers, allows the heat conduction to the unreacted areas.^[37,42] The thermal diffusion is directly proportional to the thermal conductivity, which will vary with temperature,^[43] and in the case of the multilayers will be anisotropic.^[44] The introduction of growth defects normal to the layers (y -direction) will impact the thermal conductivity of the system.^[23,45] Hence, the thermal diffusivity normal to the trenches (x -direction) will be affected. Especially, the pinholes observed in the microstructure will act as a barrier for thermal diffusion, limiting the heat transfer to the unreacted areas, thus reducing the velocity of propagation of the reaction.

4.2.1. Analytical Approach

In most analytical models of the reaction propagation in RMS, the atomic and thermal diffusion are factors which influence the velocity of propagation. While the atomic diffusion will determine how fast the atoms diffuse normal to the layers, the thermal diffusion determines how rapidly the produced heat is conducted along the length of the foil.^[42] Armstrong and Koszykowski assumed that atomic and thermal diffusion can be treated as 1D processes to predict propagation velocities in reactive multilayers.^[46]

$$V^2 = \frac{3A \exp\left(-\frac{E_a}{RT_m}\right) RT_m^2 \lambda^2}{\delta^2 E_a (T_m - T_0)} \quad (1)$$

where A is an Arrhenius prefactor, E_a is the activation energy, R is the gas constant, δ is $\frac{1}{4}$ of the bilayer thickness, T_0 is the initial temperature, T_m is the maximum temperature obtained during propagation, and λ is the average thermal diffusivity.

If we consider these parameters to calculate the velocity of propagation for a system with a defined bilayer thickness and defined atomic composition, it is possible to assume that for the ignited samples δ , E_a , and A are constants.^[43] The equation be rearranged as follows:

$$\frac{V^2(T_m - T_0)\delta^2 E_a}{T_m^2 \lambda^2 * 3AR} = \exp(-E_a/RT_m) \quad (2)$$

By replacing these constants with a K factor with dimensions [K ms^{-1}], the equation is reduced to

$$\ln\left[\frac{V^2(T_m - T_0)}{K\lambda^2 * T_m^2}\right] = -\frac{E_a}{R} * \frac{1}{T_m} \quad (3)$$

We will assume K as constant and by taking the natural logarithm we make this argument nondimensional. To simplify this analysis, as the growth defects are formed at the flanks of the trenches and the width of them is constant for all the samples, we consider each trench as an area of concentration of growth defects, hence as a big barrier for the thermal transfer. Additionally, we assume that the growth defects at the trenches impact only on the thermal diffusivity and on the maximum temperature. The pinholes perpendicular to the layers act as a barrier for heat transfer; therefore, thermal diffusion in the direction parallel to the layers and perpendicular to the growth defects will be affected. **Figure 8** is a schematic of the concentration of pinholes within the trenches, which subsequently influences heat transfer as the reaction propagates perpendicular to the growth defects (x -direction).

Considering that the DSC analysis did not show a significant difference between the enthalpy calculated for the reference sample and the RMS-T, we assume that the activation energy for the reference samples and the RMS-T is the same. This assumption allows us to present the following equation:

$$\frac{\ln(V_r^2(T_{rm} - T_0)/K\lambda^2 * T_{rm}^2)}{(1/T_{rm})} = \frac{\ln(V_x^2(T_{xm} - T_0)/K(\alpha\lambda)^2 * T_{xm}^2)}{(1/T_{xm})} \quad (4)$$

where V_r and T_{rm} are the velocity and temperature of the reference sample and V_x and T_{xm} are the values from the RMS-T. Various analytical models concerning self-propagating reactions have relied on a constant thermal diffusivity,^[20,43,44] hence, in the following equation it will be replaced by 1, same as K . For the RMS-T, λ will be affected for a factor α , which is a nondimensional factor representing the impact of the growth defects on the thermal diffusivity and therefore on the velocity of propagation. In order to obtain V_x in function of V_r , the equation can be rearranged as follows:

$$\frac{T_{rm}}{T_{xm}} \ln\left[\frac{V_r^2(T_{rm} - T_0)}{T_{rm}^2}\right] - \ln\left[\frac{(T_{xm} - T_0)}{(\alpha)^2 T_{xm}^2}\right] = \ln V_x^2 \quad (5)$$

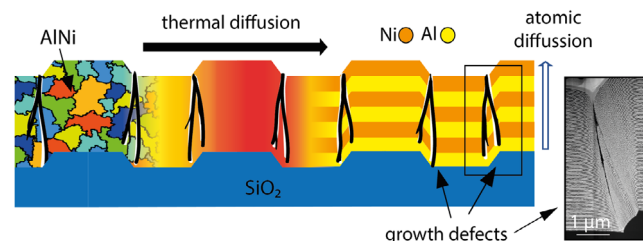


Figure 8. Schematic of the self-propagating reaction of RMS-T in x -direction.

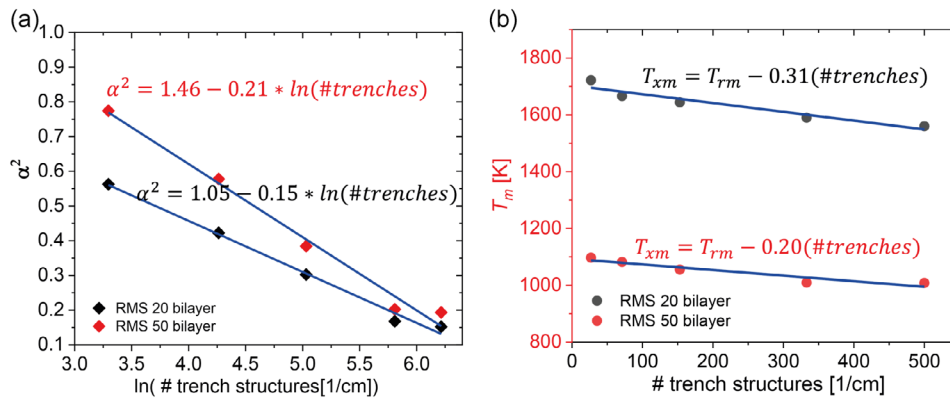


Figure 9. a) Linear fit of α^2 (impact in the thermal diffusion coefficient) versus natural logarithm of the number of trench structures per centimeter (#trenches). b) Linear fit of T_m versus the number of trench structures per centimeter (#trenches).

$$V_x^2 = \frac{[V_r^2(T_{rm} - T_0)/T_{rm}^2]^{T_{rm}/T_{xm}}}{(T_{mx} - T_0)/\alpha^2 T_{xm}^2} \quad (6)$$

$$V_x = \frac{[V_r^2(T_{rm} - T_0)]^{T_{rm}/2T_{xm}}}{[(T_{xm} - T_0)/\alpha^2 T_{xm}^2]^{1/2}} \quad (7)$$

If we replace the experimental values of velocity and temperature of the RMS-T, we can calculate α . T_0 for the experiments is room temperature. Then the obtained values can be related to the number of trench structures because it is directly related with the number of growth defects in the system. Figure 9a depicts a linear dependency of α^2 on the natural logarithm of the number of trenches per cm, whereas Figure 9b illustrates the linear dependency of T_m on the number of trenches.

The values of the slopes and intercepts, along with their respective errors, are provided in Table 2. The low errors indicate that the number of trench structures will dictate the values of α and T_m . Thus, it can be inferred that the observed growth defects are decisive factors for thermal transport and determine the velocity of propagation. To simplify the analysis, only the impact on thermal diffusivity was incorporated into the analytical model. It is important to acknowledge that the analytical models employed are oversimplified, assuming composition-independent diffusivities and temperature-independent material properties. In reality, the process is far more intricate, involving various variables.

If the mean values of α^2 and T_m are replaced in Equation (7), we obtain the propagation velocities for both systems. The calculated values are plotted in Figure 10.

The plot of velocity of propagation as a function of the number of trenches will be useful to design the substrate surface

Table 2. Values of the slopes and intercepts, with the respective errors obtained from the linear fit of α^2 and T_m versus the trench structures.

Λ	α^2		T_m	
	Slope	Intercept	Slope	Intercept
20 nm	-0.15 ± 0.007	1.05 ± 0.038	-0.31 ± 0.054	1703.6 ± 15.02
50 nm	-0.21 ± 0.014	1.46 ± 0.072	-0.20 ± 0.037	1093.1 ± 10.01

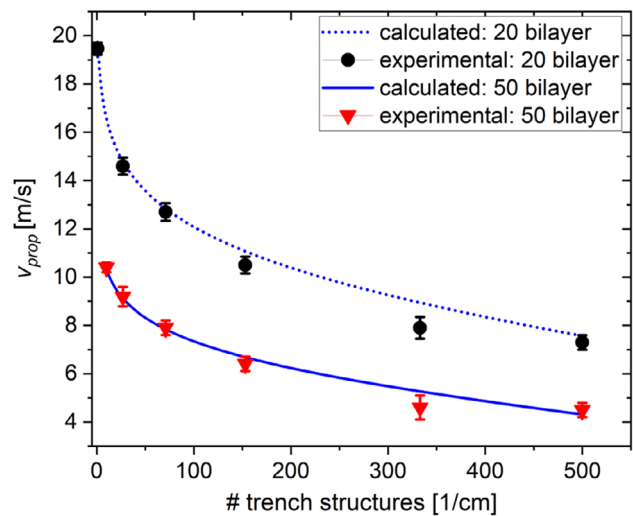


Figure 10. Calculated propagation velocity of the RMS-T in relation to the number of trench structures.

according to the desired velocity. Further investigation into the heat transfer mechanisms and the atomic diffusion are necessary to enhance the performance of the analytical model.

5. Conclusions

This work began with the hypothesis that growth defects can be used to control the temperature and propagation velocity of self-propagating reactions. Substrates with periodic 2D structures enabled the introduction of systematically distributed growth defects in RMS-T. Inhomogeneities in the bilayer and parallel pinholes were produced due to the sputtering process along etched trenches in silicon. As they act as hurdles for the thermal diffusion along the propagation path, it was possible to show that there is a direct relation between the number of growth defects, maximum temperature, and propagation velocity. DSC measurements revealed that the enthalpy is not affected by the growth defects, and XRD analysis shows the complete reaction of the parent materials in B2-AlNi phase. Based on

the experimental data, we propose a simplified analytical model that allows for the evaluation of the impact of the generated growth defects on thermal diffusivity. Furthermore, it has been demonstrated that the propagation velocity of Al/Ni multilayers, featuring bilayer thicknesses of 50 and 20 nm on silicon, can be tailored in response to the number of trench structures on the substrate. This allows the velocity of propagation to be adjusted in the range from 7.3 to 19.4 m s⁻¹ for the RMS-T with 20 nm bilayer thickness and from 4.5 to 10.4 m s⁻¹ for the RMS-T with 50 nm bilayer thickness, without changing the atomic composition or the bilayer thickness of the system. This is useful for the simultaneous production of reactive systems with different characteristics. A deeper investigation is required to quantify the local influence of the growth defects on the kinetics of the reaction and heat release.

Acknowledgements

The work was supported by the Deutsche Forschungsgemeinschaft—project 426206394 (DFG, grant Scha 632/29) and project: 426362670 (DFG, grant Scha 632/30) and grant Scha 632/27, “DFG-Gerätezentrum”). K.J. and H.B. acknowledge financial support from the German Research Foundation (DFG) through grant BA 6161/1-1. S.R. and I.G. acknowledge financial support from the German Research Foundation (DFG) through grant GA 1721/3-1 and 3-2. M.G. and J.B. acknowledge financial support from the German Research Foundation (DFG) through grant BE 3198/7 (project: 426339810). N.P. and R.S. acknowledge financial support from the German Research Foundation (DFG) through grant SCHW 855/8. This work was also supported by the free state of Thuringia under grants 2015 FGI 0025 305 (FastXRD) and B715-10009 (BioMacroNano2020), all co-financed by the European Union within the framework of the European Regional Development Fund (ERDF). Joachim Döll from the Center of Micro- and Nanotechnology (ZMN), a DFG-funded core facility at TU Ilmenau, is gratefully acknowledged for his professional help in the deposition of the samples. This work contains results obtained from experiments performed at the Ernst Ruska-Centre (ER-C) for Microscopy and Spectroscopy with Electrons at the Forschungszentrum Jülich (FZJ) in Germany [https://doi.org/10.17815/jlsrf-2-68]. The ER-C beam-time access was provided via the DFG Core Facility Project (FZJ)_IEK- 2_PN1).

Open Access funding enabled and organized by Projekt DEAL.

Conflict of Interest

The authors declare no conflict of interest.

Data Availability Statement

The data that support the findings of this study are available from the corresponding author upon reasonable request.

Keywords

2D structured surface, Al/Ni multilayers, reactive multilayer systems, self-propagating reactions, thermal diffusion, velocity of propagation

Received: December 29, 2023

Revised: May 27, 2024

Published online: June 10, 2024

- [1] D. P. Adams, R. V. Reeves, M. J. Abere, C. Sobczak, C. D. Yarrington, M. A. Rodriguez, P. G. Kotula, *J. Appl. Phys.* **2018**, 124, 95105.
- [2] G. M. Fritz, S. J. Spey, M. D. Grapes, T. P. Weihs, *J. Appl. Phys.* **2013**, 113, 14901.
- [3] J. P. McDonald, V. C. Hodges, E. D. Jones, D. P. Adams, *Appl. Phys. Lett.* **2009**, 94, 34102.
- [4] A. B. Mann, A. J. Gavens, M. E. Reiss, D. van Heerden, G. Bao, T. P. Weihs, *J. Appl. Phys.* **1997**, 82, 1178.
- [5] A. J. Gavens, D. van Heerden, A. B. Mann, M. E. Reiss, T. P. Weihs, *J. Appl. Phys.* **2000**, 87, 1255.
- [6] K. J. Blobaum, D. van Heerden, A. J. Gavens, T. P. Weihs, *Acta Mater.* **2003**, 51, 3871.
- [7] M. Glaser, S. Matthes, J. Hildebrand, J. Pierre Bergmann, P. Schaaf, *Mater. Des.* **2023**, 226, 111561.
- [8] T. A. Baginski, S. L. Taliaferro, W. D. Fahey, *J. Propul. Power* **2001**, 17, 184.
- [9] T. A. Baginski, T. S. Parker, W. D. Fahey.
- [10] T. W. Barbee, R. L. Simpson, A. E. Gash, J. H. Satcher, Nano-Laminate-Based Igniters.
- [11] C. J. Morris, B. Mary, E. Zakar, S. Barron, G. Fritz, O. Knio, T. P. Weihs, R. Hodgins, P. Wilkins, C. May, *J. Phys. Chem. Solids* **2010**, 71, 84.
- [12] D. P. Adams, *Thin Solid Films* **2015**, 576, 98.
- [13] M. Glaser, S. Matthes, S. S. Riegler, J. Hildebrand, J. P. Bergmann, P. Schaaf, I. Gallino, in *Characterization of Plastic-Metal Hybrid Composites Joined by Means of Reactive Al/Ni Multilayers: Evaluation of Occurring Thermal Regime*, ilmedia, Ilmenau April **2023**.
- [14] A. Wang, I. Gallino, S. S. Riegler, Y.-T. Lin, N. A. Isaac, Y. H. Sauni Camposano, S. Matthes, D. Flock, H. O. Jacobs, H.-W. Yen, P. Schaaf, *Mater. Des.* **2021**, 206, 109790.
- [15] D. Lee, G.-D. Sim, K. Xiao, J. J. Vlassak, *J. Phys. Chem. C* **2014**, 118, 21192.
- [16] S. Danzi, V. Schnabel, J. Gabl, A. Sologubenko, H. Galinski, R. Spolenak, *Adv. Mater. Technol.* **2019**, 4, 1800468.
- [17] G. M. Fritz, H. Joress, T. P. Weihs, *Combust. Flame* **2011**, 158, 1084.
- [18] S. Q. Arlington, G. M. Fritz, T. P. Weihs, *Annu. Rev. Mater. Res.* **2022**, 52, 219.
- [19] R. Liu, C. Gao, A. Hou, S. Wang, *J. Mater. Process. Technol.* **2023**, 321, 118167.
- [20] S. Danzi, V. Schnabel, X. Zhao, J. Käch, R. Spolenak, *Appl. Phys. Lett.* **2019**, 114, 183102.
- [21] G. M. Fritz, J. A. Grzyb, O. M. Knio, M. D. Grapes, T. P. Weihs, *J. Appl. Phys.* **2015**, 118, 135101.
- [22] S. Danzi, M. Menétrey, J. Wohllwend, R. Spolenak, *ACS Appl. Mater. Interfaces* **2019**, 11, 42479.
- [23] S. Q. Arlington, J. Chen, T. P. Weihs, *ACS Sustainable Chem. Eng.* **2020**, 8, 17262.
- [24] B. Liu, X. Yu, X. Jiang, Y. Qiao, L. You, Y. Wang, F. Ye, *Appl. Surf. Sci.* **2021**, 546, 149098.
- [25] Y. H. Sauni Camposano, S. S. Riegler, K. Jaekel, J. Schmauch, C. Pauly, C. Schäfer, H. Bartsch, F. Mücklich, I. Gallino, P. Schaaf, *Appl. Sci.* **2021**, 11, 9304.
- [26] K. Jaekel, Y. H. Sauni Camposano, S. Matthes, M. Glaser, P. Schaaf, J. P. Bergmann, J. Müller, H. Bartsch, *J. Mater. Sci.* **2023**, 58, 12811.
- [27] K. Jaekel, H. Bartsch, J. Muller, Y. H. S. Camposano, S. Matthes, P. Schaaf, in *2022 IEEE 9th Electronics System-Integration Technology Conf. (ESTC): September 13th–16th 2022*, Sibiu, Romania Conf. Proc., IEEE, Piscataway, NJ **2022**, p. 379.
- [28] H. Yesenia, S. Camposano, H. Bartsch, S. Matthes, M. Oliva-Ramirez, K. Jaekel, P. Schaaf, *Phys. Status Solidi* **2023**, 220, 2200765.
- [29] S. Matthes, M. Glaser, E. Vardo, Y. H. S. Camposano, K. Jaekel, J. P. Bergmann, P. Schaaf, *J. Mater. Sci.* **2023**, 58, 10085.

- [30] G. Teodorescu, P. D. Jones, R. A. Overfelt, B. Guo, *J. Phys. Chem. Solids* **2008**, 69, 133.
- [31] M. Adachi, Y. Yamagata, M. Watanabe, S. Hamaya, M. Ohtsuka, H. Fukuyama, *ISIJ Int.* **2021**, 61, 684.
- [32] C. A. Schneider, W. S. Rasband, K. W. Eliceiri, *Nat. Methods* **2012**, 9, 671.
- [33] P. Panjan, A. Drnovšek, P. Gselman, M. Čekada, M. Panjan, *Coatings* **2020**, 10, 447.
- [34] M. Salvalaglio, R. Backofen, A. Voigt, *Phys. Rev. B* **2016**, 94, 235432.
- [35] N. Bishop, *J. Astron. Telesc. Instrum. Syst.* **2019**, 5, 021005-1.
- [36] R. Knepper, M. R. Snyder, G. Fritz, K. Fisher, O. M. Knio, T. P. Weihs, *J. Appl. Phys.* **2009**, 105, 83504.
- [37] T. P. Weihs, Fabrication and characterization of reactive multilayer films and foils.
- [38] S. Jayaraman, O. M. Knio, A. B. Mann, T. P. Weihs, *J. Appl. Phys.* **1999**, 86, 800.
- [39] J. C. Trenkle, J. Wang, T. P. Weihs, T. C. Hufnagel, *Appl. Phys. Lett.* **2005**, 87, 153108.
- [40] C. Michaelsen, K. Barmak, T. P. Weihs, *J. Phys. D: Appl. Phys.* **1997**, 30, 3167.
- [41] I. Sraj, M. Vohra, L. Alawieh, T. P. Weihs, O. M. Knio, *J. Nanomater.* **2013**, 2013, 198096.
- [42] M. D. Grapes, T. P. Weihs, *Combust. Flame* **2016**, 172, 105.
- [43] J. K. Carson, *Int. J. Thermophys.* **2022**, 43, 108.
- [44] L. Alawieh, O. M. Knio, T. P. Weihs, *J. Appl. Phys.* **2011**, 110, 13509.
- [45] R. L. Xu, M. Muñoz Rojo, S. M. Islam, A. Sood, B. Vareskic, A. Katre, N. Mingo, K. E. Goodson, H. G. Xing, D. Jena, E. Pop, *J. Appl. Phys.* **2019**, 126, 185105.
- [46] R. Armstrong, *Combust. Sci. Technol.* **1990**, 71, 155.
- [47] Y. H. Sauni Camposano, Controlling propagation velocity in Al/Ni reactive multilayer systems by periodic 2D surface structuring, **2023**, <https://zenodo.org/records/10436346> (accessed: December 2023).